ACS Photonics

pubs.acs.org/journal/apchd5

Article

On-Chip Mid-Infrared Supercontinuum Generation from 3 to 13 μm Wavelength

Miguel Montesinos-Ballester,*,# Christian Lafforgue,# Jacopo Frigerio, Andrea Ballabio, Vladyslav Vakarin, Qiankun Liu, Joan Manel Ramirez, Xavier Le Roux, David Bouville, Andrea Barzaghi, Carlos Alonso-Ramos, Laurent Vivien, Giovanni Isella, and Delphine Marris-Morini

Cite This: *ACS Photonics* 2020, 7, 3423−3429

Read Online

ACCESS | Metrics & More | Article Recommendations

ABSTRACT: Midinfrared spectroscopy is a universal way to identify chemical and biological substances. Indeed, when interacting with a light beam, most molecules are responsible for absorption at specific wavelengths in the mid-IR spectrum, allowing to detect and quantify small traces of substances. On-chip broadband light sources in the mid-infrared are thus of significant interest for compact sensing devices. In that regard, supercontinuum generation offers a mean to efficiently perform coherent light conversion over an ultrawide spectral range, in a single and compact device. This work reports the experimental demonstration of on-chip two-octave supercontinuum generation in the mid-infrared wavelength, ranging from 3 to 13 μm (that is larger than 2500 cm^{-1}) and covering almost the full transparency window of germanium. Such an ultrawide spectrum is achieved thanks to the unique features of Ge-rich graded SiGe waveguides, which allow second-order dispersion tailoring and low propagation losses over a wide wavelength range. The influence of the pump wavelength and power on the supercontinuum spectra has been studied. A good agreement between the numerical simulations and the experimental results is reported. Furthermore, a very high coherence is predicted in the entire spectrum. These results pave the way for wideband, coherent, and compact mid-infrared light sources by using a single device and compatible with large-scale fabrication processes.

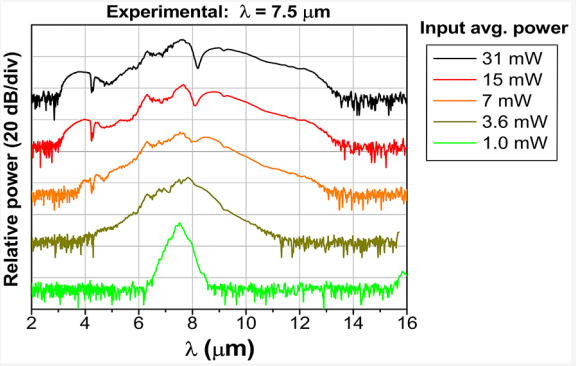

KEYWORDS: *supercontinuum, mid-infrared, nonlinear, integrated circuits, silicon, germanium*

The mid-infrared (mid-IR) wavelength range has attracted substantial attention in the past two decades due to its great importance for spectroscopy and sensing applications, as a wide variety of molecules features strong vibrational and rotational resonances in this spectral region.[1] Further applications are related to free-space communications and imaging within the atmospheric transparency windows (from 3 to 5 μm and 8 to 13 μm wavelength).[2,3] Over the past decade, mid-infrared light sources, such as interband cascade lasers (ICLs)[4] or quantum cascade lasers (QCLs),[5,6] have reached an impressive level of technological maturity. Recently, strain or lattice engineering of group IV materials has also shown to be an exciting emerging solution for silicon-compatible mid-IR lasers.[7,8] Even though these technologies can cover the wide mid-IR spectrum range, the wavelength range covered by a single device is strongly limited. While different techniques have been proposed to extend this wavelength range, based on laser arrays[9,10] or external cavity lasers,[11] the use of nonlinear optical effects is a promising alternative solution, enabling light emission over an ultrawide spectral range within a single and compact photonic device.[12−15] In this context, integrated supercontinuum generation (SCG) is extensively studied as a mean to provide broadband and coherent light. SCG sources present a compelling interest for the parallel detection of a myriad of molecules in a single, compact, and reliable system, at a reduced cost. Achieving an efficient SCG requires an integrated platform with (i) low propagation losses, (ii) a strong modal nonlinear coefficient, and (iii) a tailored modal dispersion.

Ultrawide SCG has been demonstrated using specifically engineered optical fibers. For instance, a wide spectral range from 1.4 to 13.3 μm wavelength has been covered thanks to a high nonlinear chalcogenide step-index fiber, pumped at 6.3 μm with 2.29 MW peak power,[16] and a 2 to 16 μm wavelength

Received: August 4, 2020
Published: November 11, 2020

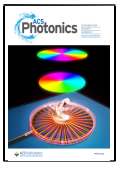

https://dx.doi.org/10.1021/acsphotonics.0c01232
ACS Photonics 2020, 7, 3423−3429

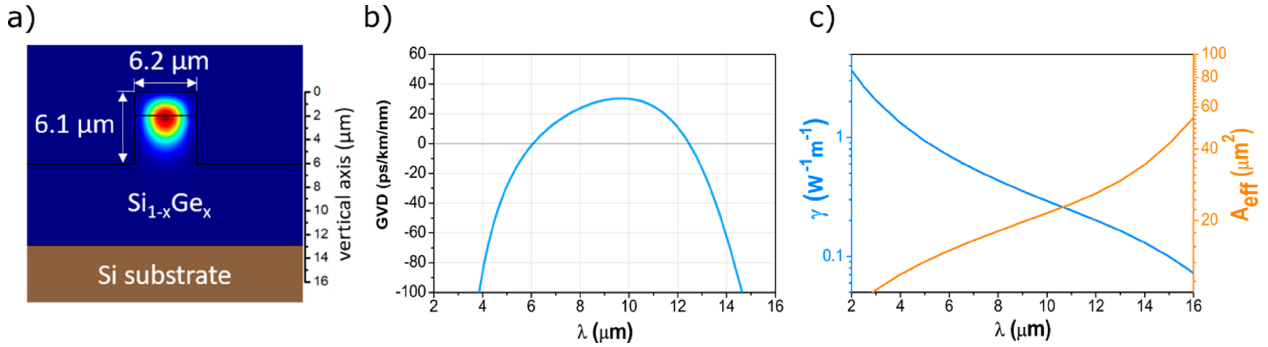

Figure 1. Waveguide properties. (a) Schematic of the waveguide profile and the field distribution of the fundamental TE mode at 8.5 μm wavelength. (b) GVD for TE polarization mode. (c) Modal nonlinear coefficient (left y-axis) and effective area (right y-axis) as a function of the wavelength.

spectrum broadening has been achieved with a low-loss telluride fiber, pumped at 7 μm wavelength with 11.5 mW average power.[17] On another hand, in terms of photonics integration, silicon (Si) photonics presents strong advantages, as it is based on a mature and large-scale fabrication technology. Hence, SCG has been demonstrated on Si-on-insulator,[18,19] Si-on-sapphire,[20] silicon nitride (SiN),[21−23] and germanium (Ge)-based waveguides.[24−26] Interestingly, Ge-rich graded SiGe waveguides have been proposed as a promising solution for mid-IR photonic circuits in which low-loss devices have been experimentally demonstrated for a large wavelength range.[27] The use of SiGe graded-index layers is a unique feature that minimizes the overlap with Si substrate, thus, enabling the use of long-wave mid-IR wavelengths above Si multiphonon absorption (starting at 8.5 μm wavelength). Moreover, a high material quality is obtained, providing low threading dislocation density (TDD) and therefore allowing low propagation losses over an unprecedented mid-IR wavelength range. Furthermore, the use of SiGe graded-index layers brings a simple yet effective approach for waveguide dispersion engineering,[28] while it also permits to pull the optical mode toward the Ge-rich area, to benefit from a larger nonlinear refractive index.[29] It is also remarkable that this platform is compatible with large-scale fabrication processes.

A two-octave SCG in the mid-IR regime is demonstrated in this work, providing a compact and coherent light source that covers an unprecedented wavelength range, from 3 to 13 μm wavelength. To that end, this work takes advantage of the remarkable features of such a Ge-rich graded SiGe platform. Noticeably, numerical simulations are provided, showing a good agreement with the experimental results for different pump wavelengths and injected optical power values, also predicting a high coherence in the entire spectrum. Therefore, these results pave the way for the realization of wideband and coherent light sources, by using a single chip-scale compact device. For instance, this demonstration offers a great opportunity to perform on-chip mid-IR spectroscopy sensing of a significant large number of molecules, thus, having a compelling interest in many high-impact applications.

RESULTS

Design and Fabrication of Graded-Index SiGe Platform. The fabricated waveguides leverage on a Ge-rich graded SiGe platform[30] where a constant composition layer of $Si_{0.2}Ge_{0.8}$ is deposited on top of an 11 μm thick $Si_{1-x}Ge_x$ buffer, with the Ge fraction x linearly increasing from $x = 0$ (pure Si) to $x = 0.79$.[27] The photonic circuit fabrication relies on low-energy plasma-enhanced chemical vapor deposition (LEPECVD) for the SiGe layer growth, followed by laser lithography and inductively coupled plasma-reactive ion etching (ICP-RIE) for waveguide fabrication. This platform provides a smooth transition from the Si substrate to the Ge-rich SiGe alloy, thus, minimizing the TDD due to lattice mismatch. Interestingly, since the refractive index increases linearly with the Ge content, the optical mode is pushed toward the top layer, achieving a tight mode confined in the Ge-rich region and far from the Si substrate, where the multiphonon excitation is responsible for absorption at wavelengths longer than 8.5 μm.[31] Moreover, the nonlinear refractive index n_2 reaches the maximum value in the Ge-rich region, thus, maximizing the modal nonlinear coefficient γ. Finally, another remarkable aspect of the graded index platform is its favorable anomalous dispersion condition over a broad wavelength range, thanks to the combination of the gradient effect in the vertical direction together with the intrinsic low material dispersion in the mid-IR.[28,32]

As it is illustrated in Figure 1a, the waveguides considered in this work are 6.2 μm wide with a 6.1 μm etching depth. Single mode operation is achieved in TE polarization for wavelengths longer than 6.5 μm. Propagation losses between 0.5 and 1.2 dB/cm for wavelengths below 8 μm and lower than 3 dB/cm for wavelengths longer than 9.5 μm have been previously measured in such waveguides. The propagation loss measurement and a detailed study of its origins are reported in ref 27. To efficiently couple the incident optical beam to the chip, a pair of 50 μm wide and 1 mm long access waveguides are used as the input/output of the integrated circuit, followed by a 2 mm long linear transition to the 6.2 μm wide waveguide. The group velocity dispersion (GVD) of the fundamental TE mode has been numerically calculated and is reported in Figure 1b. For this calculation, the refractive indexes of Si and Ge are obtained by the Sellmeier equation, while the gradient index profile is calculated by a linear interpolation of Si and Ge refractive index. The effective refractive index (n_{eff}) as a function of the wavelength is calculated by a finite domain elements solver and finite difference coefficient method is used to obtain the second derivative to calculate the GVD. Low and flat anomalous dispersion is achieved over a large mid-IR wavelength, ranging from 6 to 13 μm. Finally, the modal nonlinear coefficient $\gamma = \omega_0 n_2/cA_{eff}$ is reported in Figure 1c, where ω_0 is the pump pulsation, A_{eff} is the effective area obtained through a finite difference eigenmode software, c is the light speed, and n_2 is the nonlinear Kerr refractive index, taken to be 1×10^{-17} m^2/W for the wavelength range under

https://dx.doi.org/10.1021/acsphotonics.0c01232
ACS Photonics 2020, 7, 3423−3429

study.[29] As we can see in Figure 1c, the nonlinear coefficient varies by more than an order of magnitude depending on the wavelength, mainly due to the variation of the effective area.

SCG Experimental Characterization. The experimental setup shown in Figure 2 is used to demonstrate SCG in the mid-IR range. A femtosecond laser emits pulses with a duration of 220 fs and a repetition rate of 1 MHz. The pulses wavelength can be selected in a wide range, thanks to an optical parametric amplifier (OPA) system, and are coupled in and out of the photonic circuit by butt coupling, using a pair of aspheric ZnSe lenses. Then, the output beam is sent to a monochromator followed by a Mercury Cadmium Telluride (MCT) detector to construct the output spectra.

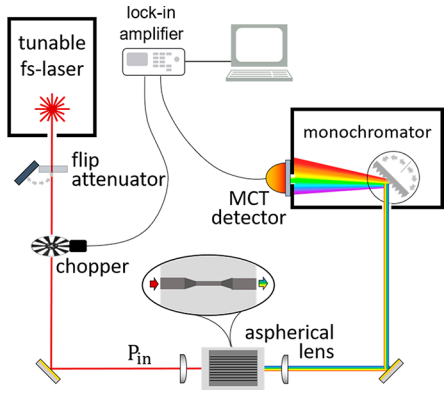

Figure 2. Characterization setup scheme used for the SCG experiments. A tunable femtosecond pulse is coupled into the waveguide and the output spectrum is obtained for different pump power values and wavelengths.

To evaluate the influence of the pump optical power on the SCG, mid-IR optical attenuators are added at the output of the femtosecond laser. The average input power before coupling to the waveguide (P_{in}) is measured with a broadband, high-power detector. To examine the influence of the pump wavelength in the SCG, three different pump wavelengths have been selected in the anomalous dispersion regime: 7.5, 8.5, and 9.4 μm. It must be noted that, since the maximum power delivered by the femtosecond laser decreases when the wavelength increases, the three different pump wavelengths have been selected to provide a good compromise between the delivered power and the anomalous dispersion condition.

SCG Measurements. Experimental SCG results on 5.5 mm-long waveguides are reported in Figure 3a,b. For a pump wavelength of 7.5 μm, the output spectrum widely extends over two octaves, from 3 to 13 μm (at −30 dB of the maximum value) for average input power values before coupling in the waveguide higher than 15 mW (Figure 3a). For the pump wavelength of 8.5 μm (Figure 3b) the SCG is more efficient, as an average input power of 8 mW is required to achieve an output spectrum extending from 3 to 13 μm. It must be noted that, since the characterization setup is based on a free-space configuration, absorption lines of the different atmospheric molecules are distinguishable in the experimental spectra. As an example, in Figure 3a,b the absorption peak of carbon

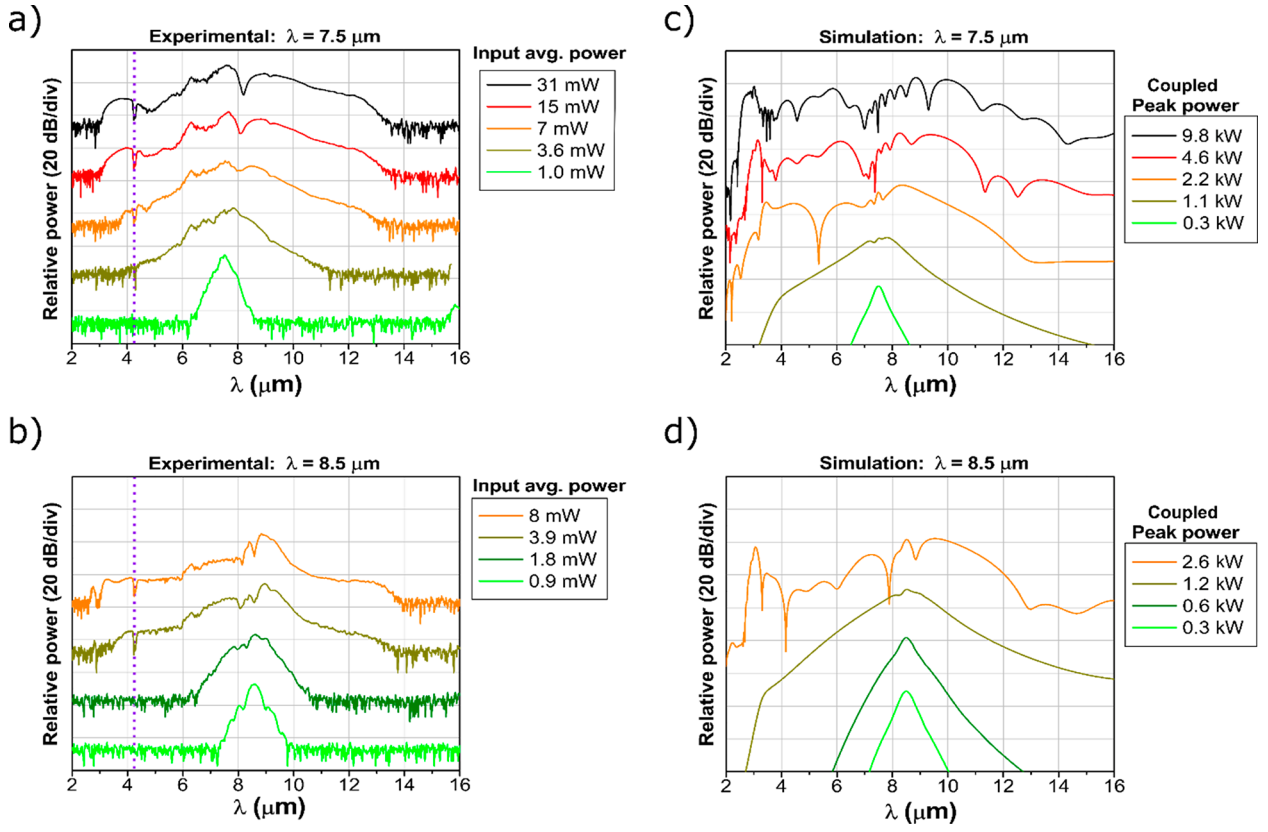

Figure 3. Experimental and simulated SCG. (a, b) Output relative power experimentally measured in a 5.5 mm long waveguide for different input average power values and input pump wavelengths of 7.5 and 8.5 μm. For the sake of clarity, each trace has been shifted by 30 dB. A vertical dashed line at 4.2 μm wavelength is reported corresponding to CO_2 atmospheric absorption. (c, d) Simulated SCG spectra for the different pump wavelengths and the corresponding peak power value, calculated from the average input power and assuming 14 dB coupling losses.

https://dx.doi.org/10.1021/acsphotonics.0c01232
ACS Photonics 2020, 7, 3423−3429

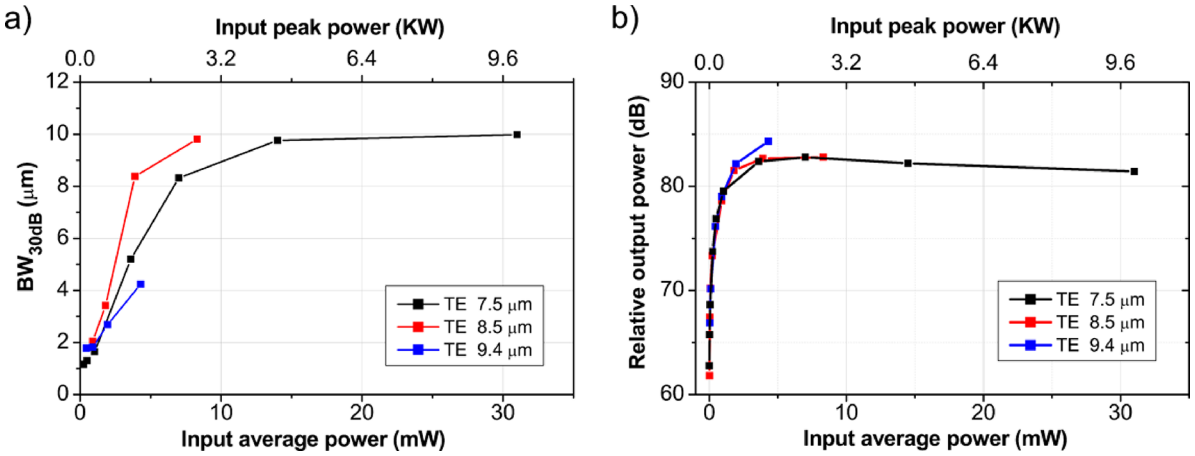

Figure 4. Experimental SCG efficiency. (a) Bandwidth at −30 dB of the maximum value. (b) Integrated output power detected. The values are plotted as a function of the average input power (bottom *x*-axis) or the calculated input peak power (top *x*-axis) for different pump wavelengths in TE polarization: 7.5, 8.5, and 9.4 μm.

dioxide near 4.2 μm is clearly visible, highlighted by a dashed vertical line.

The influence of pump wavelength and pump power on the −30 dB-bandwidth is plotted in Figure 4a. Measurements are reported for wavelengths of 7.5, 8.5, and 9.4 μm. It must be noted that, since the maximal power delivered by the laser decreases with longer wavelengths, the bandwidth at 9.4 μm pump wavelength is limited to 4 μm. However, at 7.5 and 8.5 μm pump wavelength, a maximal bandwidth of 10 μm is achieved. Interestingly, at low input power values, the optimal conversion efficiency is experimentally obtained at 8.5 μm (red data points). Furthermore, the integrated output power is reported in Figure 4b for the different pump wavelengths. A slight decay of the output power as a function of the input power is observed when the input peak power achieves values higher than 3 kW. Since the pump wavelength is beyond the limit for 2 and 3 photons absorption of SiGe waveguides, it is expected that this decay is in fact explained by the spectral limitation of the waveguide and experimental setup at large wavelengths, as described below, meaning that the signal generated on-chip reaches a wavelength range broadening even larger than 10 μm, that is not experimentally measured.

SCG Simulation and Modeling. Numerical modeling has been implemented to have a better understanding of the experimental results and to get insights of the SCG limiting factors. The modeling is based on the resolution of the generalized nonlinear Schrödinger equation (GNLSE)[22,33] by using a 4-order Runge−Kutta algorithm.[34] For such simulations, the pump pulse shape is assumed to be a squared hyperbolic secant (sech^2), the nonlinear Kerr refractive index[29] (n_2) is taken to be 1×10^{-17} m^2/W, and the dispersion profile is calculated through an eigenmode solver software (Figure 1b). The Raman contribution is expected to be very low in the wavelength range under study and is neglected in the theoretical model. Finally, as there is no currently available experimental data for propagation losses beyond 11.2 μm and below 5 μm wavelength, the values experimentally measured at 11.2 and 5 μm are assumed to be a good approximation outside of this range.

Simulated SCG spectra for the different pump wavelengths and for a 5.5 mm long waveguide are reported in Figure 3c,d. The wavelength range has been chosen to be the same as in the experiments, i.e. from 2 to 16 μm. The peak power values used for the simulations are consistent with the average optical power values measured in the experiments (Figure 3a,b) when taking into account the laser pulse repetition rate and 14 dB free-space to waveguide coupling losses, which is compatible with insertion losses estimated by cut-back method. Interestingly, the shapes of the simulated spectra for the different pump wavelengths and power values are in good agreement with the experimental data. For a 7.5 μm pump wavelength, a wide spectrum from 3 to 13 μm is obtained for a peak power of 4.6 kW (corresponding to 15 mW average input power), while at 8.5 μm pump wavelength, such a wide spectrum is obtained at 2.6 kW peak power (8 mW average power). In order to locate the dispersive waves (DW) on the generated spectrum, the integrated dispersion (β_{int}) is calculated for a 7.5 μm pump wavelength at different pump peak power values, as shown in Figure 5. The crossing with zero (horizontal dashed line)

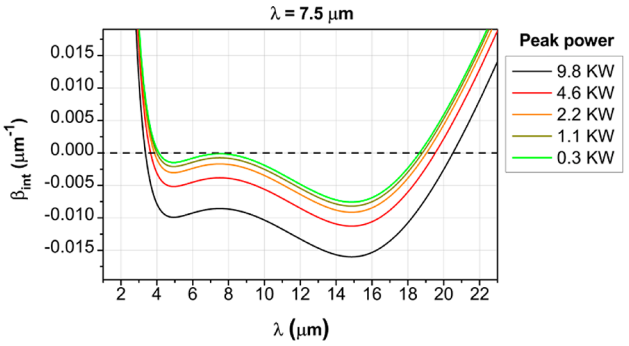

Figure 5. Integrated dispersion profile as a function of the wavelength, for a pump wavelength of 7.5 μm and different peak powers. The cross with zero indicates the phase-matching condition.

indicates the phase-matching condition that promotes the DW generation.[22] The wide anomalous dispersion profile achieved leads to a large separation of the DW from the pump wavelength (near 3.5 and 19 μm), thus, enlarging the output spectrum up to more than two octaves. The generated DW near 3.5 μm for the pump wavelength of 7.5 μm is visible in both experimental and simulated spectra (Figure 3a,c), while the noise level prevents seeing experimentally any signal beyond a 14 μm wavelength. Indeed, while the upper DW should be centered around a 19 μm wavelength, the extension

https://dx.doi.org/10.1021/acsphotonics.0c01232
ACS Photonics 2020, 7, 3423−3429

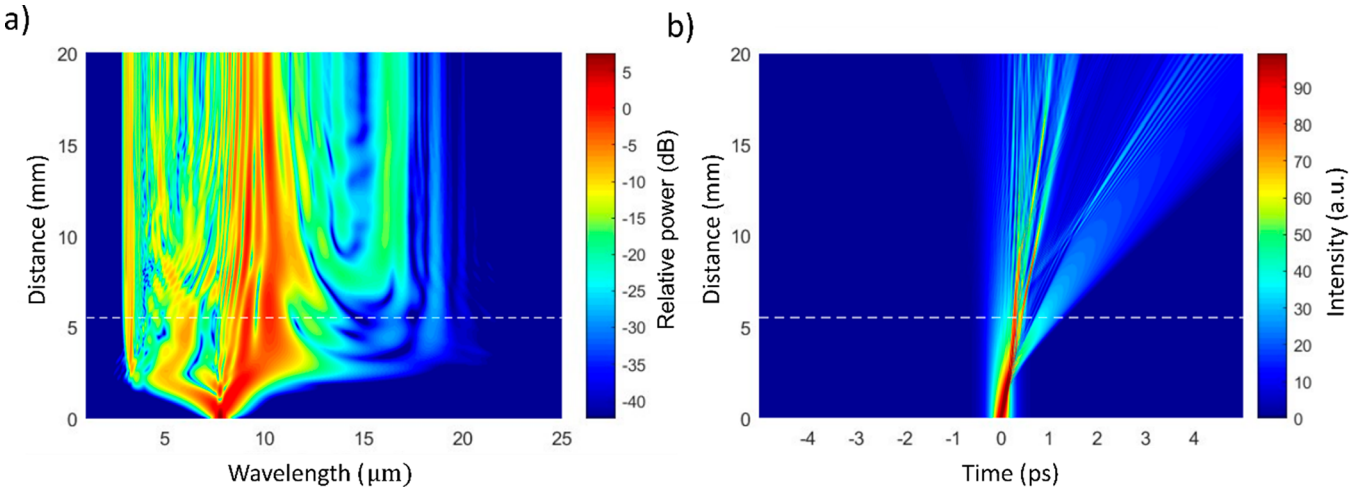

Figure 6. Pulse propagating evolution. (a) Wavelength spectrum evolution along propagation length for a pump signal at 7.5 μm wavelength with 9.8 KW peak power. A white dashed horizontal marker indicates the 5.5 mm waveguide length. (b) Corresponding temporal envelope as a function of the propagation distance.

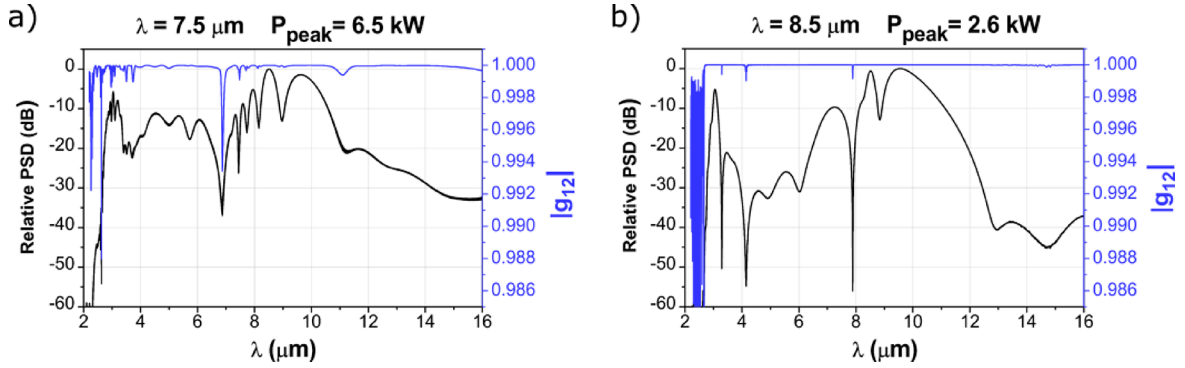

Figure 7. First-order degree of coherence plotted as a function of wavelength (blue color, right y-axis) and superposition of the 40 simulated spectra used for the statistical calculation (black color, left y-axis) after 5.5 mm propagation length and for pumps at (a) 7.5 μm wavelength and 6.5 kW peak power and (b) 8.5 μm wavelength and 2.6 kW peak power.

of the spectrum measurement at large wavelengths is limited by the contributions of (i) the atmospheric absorption above 13 μm wavelength, (ii) multiphonon absorption of Ge beyond 14 μm, and (iii) an spectral responsivity of the MCT detector (DSS-MTC(14)020L, Horiba) nearly limited at 15 μm wavelength. Therefore, as seen in Figure 4a, the SCG extension at −30 dB is limited to a maximal range value of 10 μm (from 3 to 13 μm wavelength).

To better understand the SCG in SiGe graded waveguides, the generated spectrum and temporal envelope of the propagating pulse across the waveguide length is reported in Figure 6, for a 7.5 μm wavelength and 9.8 kW peak power pump. Spectrum expansion is seen around 2 mm propagation distance (Figure 6a), corresponding to a pulse temporal compression at the same propagation length (Figure 6b). Then, the perturbation of the compressed soliton due to high order dispersion is responsible for soliton fission. The overlap of a high-power soliton bandwidth with the normal dispersion region leads to the generation of DW in the normal dispersion regime that are combined with broadband solitons. Furthermore, it can be seen, that the final spectrum is reached after 8 mm propagation length while the device under characterization are 5.5 mm long.

Finally, we investigate the coherence of the supercontinuum light source, which can be decisive for free-space communications or imaging purposes, among others.

To that end, the first order degree of mutual coherence g_{12} is calculated according to the following equation:[37]

$$g_{12}(\omega) = \frac{|\langle \tilde{A}_i^*(\omega)\tilde{A}_j(\omega)\rangle_{i\neq j}|}{\sqrt{\langle |\tilde{A}_i(\omega)|^2 |\tilde{A}_j(\omega)|\rangle^2}}$$

where the angle brackets denote an ensemble average over 40 independently generated pairs of supercontinua $\tilde{A}(\omega)$ with random input noise. The spectra $\tilde{A}(\omega)$ is obtained from the Fourier transform of the temporal pulses $A_{tot}(t)$, including the quantum shot noise such that

$$A_{tot}(t) = A_0(t) + a(t)e^{j\varphi(t)}$$

The amplitude $a(t)$ follows a Gaussian distribution with a variance value of $hf_0/(2T_e)$, as described in ref 35 and 36 (h is the Plank constant, f_0 is the central frequency of the pulse, and T_e is the sampling time). The phase $\varphi(t)$ also follows a Gaussian distribution with variance value of π.

The simulations have been performed for pump wavelengths of 7.5 and 8.5 μm, with a peak power of 6.5 and 2.6 kW, respectively, and for a propagation length of 5.5 mm. The first-order degree of mutual coherence (g_{12}) is plotted in Figure 7,

https://dx.doi.org/10.1021/acsphotonics.0c01232
ACS Photonics 2020, 7, 3423−3429

where the black line is the superposition of the 40 different spectral simulated and the blue line is the calculated g_{12}. It can clearly be seen that, when considering only the quantum shot noise, a high degree of coherence is predicted over the entire SCG

CONCLUSION

In this work we have shown the huge potential of using graded-index SiGe waveguides to exploit nonlinear processes through the experimental demonstration of SCG. First, the graded-index platform can be used for second-order dispersion engineering in a simple yet effective way while providing low propagation losses in a wide wavelength range. Furthermore, the use of Ge-rich SiGe waveguides is compatible with large-scale fabrication processes, hence, allowing compact, reliable and low-cost devices. Moreover, the use of a Ge-rich approach benefits from a large Kerr coefficient (compared to silicon) and tight confinement, thus, enhancing the nonlinear processes. Finally, this work experimentally validates the high potential of this approach to perform SCG over an unprecedented wavelength range in the mid-IR regime, achieving a two-octave expansion (covering from 3 to 13 μm wavelength). A detailed study of the phenomena is carried out, pumping at different wavelengths (7.5, 8.5, and 9.4 μm) in the anomalous dispersion regime and different input power values. Our experimental results indicate that the optimal pump wavelength is 8.5 μm, providing the maximal spectrum expansion at lower pump power. Numerical simulations show a good agreement with the experimental results. The output spectrum coherence is also numerically evaluated, demonstrating a very high first-order degree of coherence over the entire SCG range, which is crucial for many mid-IR applications. In summary, these results pave the way toward an efficient ultrawide mid-IR light source implementation by using a single and compact on-chip device.

AUTHOR INFORMATION

Corresponding Author

Miguel Montesinos-Ballester − *Centre de Nanosciences et de Nanotechnologies, Université Paris-Saclay, CNRS, 91120 Palaiseau, France;* orcid.org/0000-0003-3711-3933; Email: miguel.montesinos@c2n.upsaclay.fr

Authors

Christian Lafforgue − *Centre de Nanosciences et de Nanotechnologies, Université Paris-Saclay, CNRS, 91120 Palaiseau, France*

Jacopo Frigerio − *L-NESS, Dipartimento di Fisica, Politecnico di Milano, Polo di Como, 22100 Como, Italy*

Andrea Ballabio − *L-NESS, Dipartimento di Fisica, Politecnico di Milano, Polo di Como, 22100 Como, Italy;* orcid.org/0000-0002-2957-8717

Vladyslav Vakarin − *Centre de Nanosciences et de Nanotechnologies, Université Paris-Saclay, CNRS, 91120 Palaiseau, France*

Qiankun Liu − *Centre de Nanosciences et de Nanotechnologies, Université Paris-Saclay, CNRS, 91120 Palaiseau, France*

Joan Manel Ramirez − *Centre de Nanosciences et de Nanotechnologies, Université Paris-Saclay, CNRS, 91120 Palaiseau, France*

Xavier Le Roux − *Centre de Nanosciences et de Nanotechnologies, Université Paris-Saclay, CNRS, 91120 Palaiseau, France*

David Bouville − *Centre de Nanosciences et de Nanotechnologies, Université Paris-Saclay, CNRS, 91120 Palaiseau, France*

Andrea Barzaghi − *L-NESS, Dipartimento di Fisica, Politecnico di Milano, Polo di Como, 22100 Como, Italy*

Carlos Alonso-Ramos − *Centre de Nanosciences et de Nanotechnologies, Université Paris-Saclay, CNRS, 91120 Palaiseau, France*

Laurent Vivien − *Centre de Nanosciences et de Nanotechnologies, Université Paris-Saclay, CNRS, 91120 Palaiseau, France*

Giovanni Isella − *L-NESS, Dipartimento di Fisica, Politecnico di Milano, Polo di Como, 22100 Como, Italy;* orcid.org/0000-0001-5951-7440

Delphine Marris-Morini − *Centre de Nanosciences et de Nanotechnologies, Université Paris-Saclay, CNRS, 91120 Palaiseau, France*

Complete contact information is available at: https://pubs.acs.org/10.1021/acsphotonics.0c01232

Author Contributions

#These authors contributed equally to this work. D.M.M. and J.M.R. conceived and proposed the experiment. M.M.B. and C.L. developed the theoretical model. J.F., A.B., A.B., and G.I. carried out the epitaxial growth. M.M.B., V.V., and X.L.R. fabricated the structures. M.M.B., C.L., and Q.L. performed the measurements. M.M.B. wrote the article and discussed the results with C.L., C.A.R., G.I., L.V., and D.M.M.

Notes

The authors declare no competing financial interest.

ACKNOWLEDGMENTS

This work was supported by European Research Council (ERC) under the European Union's Horizon-2020 research and innovation program (No. 639107-InsPIRE) and EU Horizon-2020 FET microSPIRE Project No. 766955. The fabrication of the device was partially performed at the Plateforme de Micro-NanoTechnologie/C2N, which is partially funded by the "Conseil Général de l'Essonne". This work was partly supported by the French RENATECH network. PoliFAB is also acknowledged for waveguides fabrication.

REFERENCES

(1) Popa, D.; Udrea, F. Towards Integrated Mid-Infrared Gas Sensors. *Sensors* **2019**, *19*, 2076.

(2) Corrigan, P.; Martini, R.; Whittaker, E. A.; Bethea, C. Quantum cascade lasers and the Kruse model in free space optical communication. *Opt. Express* **2009**, *17*, 4355−4359.

(3) Pang, X.; Ozolins, O.; Schatz, R.; et al. Gigabit free-space multi-level signal transmission with a mid-infrared quantum cascade laser operating at room temperature. *Opt. Lett.* **2017**, *42*, 3646−3649.

(4) Vurgaftman, I.; Canedy, C. L.; Kim, C. S.; et al. Mid-infrared interband cascade lasers operating at ambient temperatures. *New J. Phys.* **2009**, *11*, 125015.

(5) Faist, J.; Capasso, F.; Sivco, D. L.; et al. Quantum cascade laser. *Science* **1994**, *264*, 553−556.

(6) Yao, Y.; Hoffman, A.; Gmachl, C. Mid-infrared quantum cascade lasers. *Nat. Photonics* **2012**, *6*, 432−439.

(7) Elbaz, A.; Buca, D.; von den Driesch, N.; et al. Ultra-low-threshold continuous-wave and pulsed lasing in tensile-strained GeSn alloys. *Nat. Photonics* **2020**, *14*, 375−382.

(8) Fadaly, E. M. T.; Dijkstra, A.; Suckert, J. R.; et al. Direct-bandgap emission from hexagonal Ge and SiGe alloys. *Nature* **2020**, *580*, 205−209.
(9) Zhou, W.; Bandyopadhyay, N.; Wu, D.; McClintock, R.; Razeghi, M. Monolithically, widely tunable quantum cascade lasers based on a heterogeneous active region design. *Sci. Rep.* **2016**, *6*, 25213.
(10) Coutard, J. G; Brun, M.; Fournier, M.; Lartigue, O.; Fedeli, F.; Maisons, G.; Fedeli, J. M; Nicoletti, S.; Carras, M.; Duraffourg, L. Volume Fabrication of Quantum Cascade Lasers on 200 mm-CMOS pilot line. *Sci. Rep.* **2020**, *10*, 6185.
(11) Vijayraghavan, K.; et al. Broadly tunable terahertz generation in mid-infrared quantum cascade lasers. *Nat. Commun.* **2013**, *4*, 2021.
(12) Silva, F.; Austin, D.R.; Thai, A.; Baudisch, M.; Hemmer, M.; Faccio, D.; Couairon, A.; Biegert, J. Multi-octave supercontinuum generation from mid-infrared filamentation in a bulk crystal. *Nat. Commun.* **2012**, *3*, 807.
(13) Vodopyanov, K. L.; Sorokin, E.; Sorokina, I. T.; Schunemann, P. G. Mid-IR frequency comb source spanning 4.4−5.4 μm based on subharmonic GaAs optical parametric oscillator. *Opt. Lett.* **2011**, *36*, 2275−2277.
(14) Villares, G.; et al. Dispersion engineering of quantum cascade laser frequency combs. *Optica* **2016**, *3*, 252−258.
(15) Guo, H.; Herkommer, C.; Billat, A.; et al. Mid-infrared frequency comb via coherent dispersive wave generation in silicon nitride nanophotonic waveguides. *Nat. Photonics* **2018**, *12*, 330−335.
(16) Petersen, C.; Møller, U.; Kubat, I.; et al. Mid-infrared supercontinuum covering the 1.4−13.3 μm molecular fingerprint region using ultra-high NA chalcogenide step-index fibre. *Nat. Photonics* **2014**, *8*, 830−834.
(17) Zhao, Z.; et al. Mid-infrared supercontinuum covering 2.0−16 μm in a low-loss telluride single-mode fiber. *Laser Photonics Rev.* **2017**, *11*, 1700005.
(18) Lau, R. K. W.; et al. Octave-spanning mid-infrared supercontinuum generation in silicon nanowaveguides. *Opt. Lett.* **2014**, *39*, 4518−4521.
(19) Leo, F.; Gorza, S.-P.; Coen, S.; Kuyken, B.; Roelkens, G. Coherent supercontinuum generation in a silicon photonic wire in the telecommunication wavelength range. *Opt. Lett.* **2015**, *40*, 123−126.
(20) Singh, N.; et al. Midinfrared supercontinuum generation from 2 to 6 μm in a silicon nanowire. *Optica* **2015**, *2*, 797−802.
(21) Grassani, D.; Tagkoudi, E.; Guo, H.; Herkommer, C.; Yang, F.; Kippenberg, T. J.; Bres, C.-S. Mid infrared gas spectroscopy using efficient fiber laser driven photonic chip-based supercontinuum. *Nat. Commun.* **2019**, *10*, 1553.
(22) Lafforgue, C.; et al. Broadband supercontinuum generation in nitrogen-rich silicon nitride waveguides using a 300 mm industrial platform. *Photonics Res.* **2020**, *8*, 352−358.
(23) Martyshkin, D.; et al. Visible-near-middle infrared spanning supercontinuum generation in a silicon nitride (Si3N4) waveguide. *Opt. Mater. Express* **2019**, *9*, 2553−2559.
(24) Sinobad, M.; et al. Mid-infrared octave spanning supercontinuum generation to 8.5 μm in silicon-germanium waveguides. *Optica* **2018**, *5*, 360−366.
(25) Sinobad, M.; et al. High Coherence at f and 2f of Mid-Infrared Supercontinuum Generation in Silicon Germanium Waveguides. *IEEE J. Sel. Top. Quantum Electron.* **2020**, *26*, 1−8.
(26) Sinobad, M.; et al. Mid-infrared supercontinuum generation in silicon-germanium all-normal dispersion waveguides. *Opt. Lett.* **2020**, *45*, 5008−5011.
(27) Montesinos-Ballester, M.; et al. Ge-rich graded SiGe waveguides and interferometers from 5 to 11 μm wavelength range. *Opt. Express* **2020**, *28*, 12771−12779.
(28) Ramirez, J. M.; et al. Ge-rich graded-index Si1-xGex waveguides with broadband tight mode confinement and flat anomalous dispersion for nonlinear mid-infrared photonics. *Opt. Express* **2017**, *25*, 6561−6567.
(29) Serna, S.; Vakarin, V.; Ramirez, J.-M.; Frigerio, J.; Ballabio, A.; Le Roux, X.; Vivien, L.; Isella, G.; Cassan, E.; Dubreuil, N.; Marris-Morini, D. Nonlinear Properties of Ge-rich $Si_{1-x}Ge_x$ Materials with Different Ge Concentrations. *Sci. Rep.* **2017**, *7*, 14692.
(30) Ramirez, J. M.; et al. Graded SiGe waveguides with broadband low-loss propagation in the mid infrared. *Opt. Express* **2018**, *26*, 870−877.
(31) Soref, R. Mid-infrared photonics in silicon and germanium. *Nat. Photonics* **2010**, *4*, 495−497.
(32) Zhang, L.; Agarwal, A. M.; Kimerling, L. C.; Michel, J. Nonlinear Group IV Photonics Based on Silicon and Germanium: From Near-Infrared to Mid-Infrared. *Nanophotonics* **2014**, *3*, 247−268.
(33) Lin, Q.; Painter, O. J.; Agrawal, G. P. Nonlinear optical phenomena in silicon waveguides: modeling and applications. *Opt. Express* **2007**, *15*, 16604−16644.
(34) Hult, J. A fourth-order Runge-Kutta in the interaction picture method for simulating supercontinuum generation in optical fibers. *J. Lightwave Technol.* **2007**, *25*, 3770−3775.
(35) Paschotta, R. Noise of mode-locked lasers (Part I): numerical model. *Appl. Phys. B: Lasers Opt.* **2004**, *79*, 153−162.
(36) Ruehl, A.; et al. Ultrabroadband coherent supercontinuum frequency comb. *Phys. Rev. A: At., Mol., Opt. Phys.* **2011**, *84*, 011806.
(37) Dudley, J. M.; Genty, G.; Coen, S. Supercontinuum generation in photonic crystal fiber. *Rev. Mod. Phys.* **2006**, *78*, 1135−1184.

https://dx.doi.org/10.1021/acsphotonics.0c01232
ACS Photonics 2020, 7, 3423−3429